Eur Biophys J (2009) 38:479–485
DOI 10.1007/s00249-008-0398-5

ORIGINAL PAPER

Modeling tumor cell shedding

S. A. Menchón · C. A. Condat

Received: 13 June 2008 / Revised: 4 December 2008 / Accepted: 14 December 2008 / Published online: 9 January 2009

Abstract Cell shedding is an important step in the development of tumor invasion and metastasis. It influences growth saturation, latency, and tumor surface roughness. In spite of careful experiments carried out using multicellular tumor spheroids (MTS), the effects of the shedding process are not yet completely understood. Using a simulational model, we study how the nature and intensity of cell shedding may influence tumor morphology and examine the dependence of the total number of shed cells with the relevant parameters, finding the ranges that maximize cell detachment. These ranges correspond to intermediate values of the adhesion, for which we observe the emergence of a rough tumor surface. They are also likely to maximize the probability of generating invasion and metastases. Using numerical values taken from experiments, we find that the shedding-induced reduction in the growth rate is not intense enough to lead to latency, except when cell adhesion is assumed to be very weak. This suggests that the presence of inhibitors is a necessary condition for the observed MTS growth saturation.

Introduction

The onset of metastasis is mediated by the shedding of cells from the primary tumor and the invasion of neighboring tissues, or by the intravasation of detached tumor cells. Since the direct in vivo observation of shedding is extremely difficult, it is useful to study this process in experimental models, such as multicellular tumor spheroids (MTS). MTS are nearly spherical aggregates of tumor cells, with no substrate for cell attachment (Hamilton 1998; Mueller-Klieser 2000). Large MTS, with diameters over approximately 500 μm, usually consist of an outer layer of proliferative cells, an intermediate layer of quiescent cells, and an inner necrotic core. An MTS usually grows monotonically until it reaches a maximum size such that the creation of new cells is exactly compensated by cell shedding at the surface (Jiang et al. 2005). Careful measurements of cell shedding from spheroid surfaces date back to at least 25 years (Landry et al. 1982). Recently, Günther et al. have investigated how polyphenols inhibit cell shedding from MTS (Günther et al. 2007), a work that could impact on future antimetastatic therapeutic courses. The interpretation of the evolution of these experimental models can be helped by the development of suitable mathematical models.

The formation of a necrotic core in an MTS is clearly influenced by the reduced amounts of oxygen and nutrients reaching its deepest layers, a problem that was carefully studied by Freyer and Sutherland (1986a, b). However, since cells in the outer rim are always exposed to high concentrations of oxygen and nutrients, these limitations cannot explain why MTS diameters usually do not reach 2 mm. Two additional mechanisms have been suggested to explain the slowdown in MTS growth: the generation of inhibitors and cell shedding. The first was proposed in the early work of Greenspan (1972, 1976), who assumed that the inhibitor changes the cell reproduction rate. Many modifications to this idea have been investigated later (Nagy 2005). Shedding, however, has received much less attention from modelers, despite its relevance to in vivo metastatic processes. We should mention a recent paper by Stein et al. (2007), who formulate a continuum model of

S. A. Menchón (✉) · C. A. Condat
CONICET and FaMAF, Universidad Nacional de Córdoba, 5000 Córdoba, Argentina
e-mail: silmenchon@gmail.com; menchon@famaf.unc.edu.ar

glioblastoma tumor spheroid invasion that includes a shedding term. They use this model to describe the observed patterns of growth and dispersion of glioblastoma tumor spheroids in a collagen gel. In this paper, on the other hand, we extend a simulational model for tumor growth to describe cell shedding by a growing MTS. Our purpose is twofold: first, to investigate if varying the cell shedding rate can alter MTS morphology, and second, if shedding can by itself stop MTS growth.

Our starting model is a nutrient competition model (Scalerandi et al. 1999; Condat et al. 2001; Menchón and Condat 2008). In this model we assume that avascular tumor growth is controlled by five rules, which are implemented directly as iterative difference equations in the computer simulations. Among other results, this procedure has led to the construction of phase diagrams that describe the various stages of cancer growth (Delsanto et al. 2000), to a description of the dynamics of tumor cords (Scalerandi et al. 2002), and to the reproduction of MRI data from real tumors (Capogrosso-Sansone et al. 2001). Lately, this approach has been used to investigate the development of subspecies and the effects of the tumor–immune system interaction (Menchón et al. 2007). Results completely in agreement with experimental data are obtained, if realistic parameters are chosen for studying tumor growth with this model (Menchón and Condat 2008). Not requiring any special symmetry, this model is more suitable than the continuum models to investigate the effects of shedding on tumor morphology, which will be the focus of our study.

Methods

A growth model

The basic growth model is as described in (Scalerandi et al. 1999). A piece of originally healthy tissue is discretized and the nutrient distribution is left to evolve. The local free nutrient concentration at node **i** at time t, $p(\mathbf{i}, t)$, satisfies the equation,

$$\frac{\partial p(\mathbf{i},t)}{\partial t} = \alpha' \sum_{j}^{NN} [p(\mathbf{j},t) - p(\mathbf{i},t)] - \gamma p(\mathbf{i},t) h(\mathbf{i},t), \tag{1}$$

where $h(\mathbf{i},t)$ is the healthy cell concentration, and α' and γ are, respectively, the nutrient diffusion rate and its absorption rate by healthy cells. The sum runs over all the nearest neighbors of the node under consideration. Once the free nutrient concentration reaches its steady state, a cancer seed is introduced and made to evolve under the following rules:

(R1) *Feeding*. Free nutrients, whose local concentration is $p(\mathbf{i}, t)$, are absorbed by cancer cells and transformed into bound nutrients, whose local concentration is $q(\mathbf{i},t)$. At low concentrations, nutrients are absorbed at a rate proportional to $p(\mathbf{i}, t)$, but, as p increases, the absorption rate saturates to a value γ_{as}. We choose the following absorption rule

$$\gamma(\mathbf{i},t) = \gamma_{as}\left[1 - e^{-\Gamma p(\mathbf{i},t)}\right]. \tag{2}$$

Here Γ is a constant affinity.

(R2) *Consumption*. Bound nutrient is consumed by **i**-node cells at a rate,

$$\beta(\mathbf{i},t) = \beta_{as}\left[1 - e^{-q(\mathbf{i},t)/c(\mathbf{i},t)}\right], \tag{3}$$

where β_{as} is the consumption rate at saturation, and the local concentration of cancer cells, $c(\mathbf{i}, t)$, has been included in the exponent because each cell can consume only its own bound nutrient. The choice of Eqs. 2 and 3 is not unique; for instance, a Michaelis–Menten form could have been chosen instead.

(R3) *Death*. If the average amount of nutrient per cell, $q(\mathbf{i}, t)/c(\mathbf{i}, t)$, falls below a given threshold Q_D, a fraction ϕ_1 of the cancer cells at node **i** dies.

(R4) *Mitosis*. If $q(\mathbf{i}, t)/c(\mathbf{i}, t)$ exceeds a mitosis threshold Q_M ($Q_M > Q_D$), a fraction ϕ_2 of the cancer cells at node **i** replicates.

(R5) *Migration*. Cancer cells migrate, at a rate α, if they sense a low local free nutrient concentration, i.e., if $p(\mathbf{i}, t)/c(\mathbf{i}, t) < P_D$, where P_D is a migration threshold.

These rules are implemented through a set of nonlinear difference equations as specified in (Scalerandi et al. 1999). Although the distribution of the cells occupying a given node point changes in time, we assume that the total node population is conserved:

$$h(\mathbf{i},t) + c(\mathbf{i},t) + d(\mathbf{i},t) = n, \tag{4}$$

where $d(\mathbf{i}, t)$ is the concentration of dead cells and n is the total cell population at any node point, assumed to be the same everywhere.

Cell shedding

To model cell shedding, we add a new rule:

(S1) After a time t_0, the tumor sheds, with a probability χ, a fraction F of those cancer cells located in a low adhesion environment (LAE). We say that a cell belonging to the **i**-th node at time t is located in an LAE if

$$\sum_{\mathbf{\Lambda}} c(\mathbf{i} + \mathbf{\Lambda}, t) < L, \tag{5}$$

where $L \leq 4$ and the sum extends over all the nearest neighbors of site **i**. A small value of L indicates that a very small number of neighbors suffice to keep the given cell attached to the main tumor. We emphasize that, while χ is the probability of occurrence of a detachment, F tells us how intense this detachment will be.

Results

In our approach, the nutrient concentrations are locally updated at each step. The time discretization step corresponds to $\Delta t = 0.001$ h. Cell concentrations are updated every 12 h. The sample we consider is a two-dimensional slab of tissue, with a discretization interval $\ell \approx 33$ μm (this corresponds to approximately 10 cells per node). The nutrient source is a vessel that runs along its lower side, where the nutrient concentration is assumed to be a constant, $p((i\ell, 0),t) = P_0$ (here i is an integer). For P_0 we take the normal glucose concentration in human sera, $P_0 = 5.5$ mM (Fang et al. 2004). Periodic boundary conditions are used at the left and right boundaries. We also assume that we have initially a healthy tissue where the nutrient distribution has reached a steady state by $t = 0$. At this time, a cancer seed is placed at the center of the lattice, and the tumor evolution starts. A parameter characterizing the tumor size is its mean radius,

$$R = N^{-1} \sum_{i=1}^{N} r_i, \tag{6}$$

where N is the number of nodes along the tumor edge and the r_i are the distances from these node points to the tumor center of mass. See Table 1 for the numerical values of the "relevant" parameters.

Since most well-fed cancer cells are expected to replicate, we selected $\phi_2 = 1$. On the other hand, not all cells are equally sensitive to nutrient depletion, and we expect that most will survive a temporary depletion; thus we took $\phi_1 = 0.25$. This is only an estimate, but the results do not depend qualitatively on the precise value we choose for this parameter. The other parameters have been chosen as follows: $\Gamma = 1$ mM, $Q_M = 1{,}000$ mM/cell, $Q_D = 100$ mM/cell, and $P_D = 2.6$ mM. At a time t_0, when the mean tumor radius reaches the value $R = 5\ell$, which roughly corresponds to the time when the first necrotic cells appear in the MTS interior, we start performing tests for LAE and counting the number of shed cells. Apart from reducing the overall tumor size, shedding induces the development of an interesting morphology. This can be observed in Fig. 1, where we show snapshots of a growing tumor, 60 days after seeding. In panel (a) we have continuous growth without shedding ($L = 0$). In the rest of the panels, the corresponding values of the thresholds are $L = 0.3$ (b), $L = 0.7$ (c), and $L = 1.2$ (d); shedding starts at a time $t_0 = 11$ days, with a probability $\chi = 0.5$. All cells found in an LAE are assumed to become detached ($F = 1$). For the lowest threshold, we observe the emergence of branches in the less well-fed (upper) tumor rim, while the lower rim remains smooth. If we increase the threshold, (c), the branches become better defined and form an almost regular pattern. Some roughness starts to be apparent at the lower edge. If the threshold is further increased, (d), the tumor becomes very craggy and some cancer cell islands can be observed.

The tumor edges in Fig. 1a–c are sharply defined. At earlier times, however, a complicated picture of islands and bridges characterizes the upper part of the tumor. This effect is stronger if the fraction F is smaller than unity. In Fig. 2 we show snapshots of a tumor with $F = 0.7$, $\chi = 0.5$, and $L = 0.7$. A "bridge" of cancer cells spans the whole upper rim. The importance of this bridge becomes evident in Fig. 2b, where only live cancer cells are shown. While the bridge is mostly formed by live cancer cells, the tumor branches consist almost exclusively of dead tumor cells.

The cumulative number M of shed cells as a function of the detachment fraction F is plotted in Fig. 3 for various times. We observe that a maximum develops for a fraction $F \approx 0.7$ of shed cells. This has a simple explanation: a very low F means that few cells are detached, while a value of F close to unity implies that the MST surface is smoothed out every time we check for detachment. This makes for regular growth, since it is rarer for cancer cells to be found in an LAE. A study of the snapshots obtained for different values of F also reveals that the number of bridges and islands reaches a maximum for the same values of the parameters that yield a peak in M. A similar behavior is observed when we plot the cumulative number of shed cells as a function of shedding probability (Fig. 4). In this case, the maximum occurs near $\chi = 0.35$. If $\chi > rsim0.6$, M is almost insensitive to changes in χ. Note also that the distances between the curves in Figs. 3 and 4 increase monotonically, indicating

Table 1 Numerical values of computational parameters

Symbol	Unit	Value	References
ℓ	μm	33	
τ	h	0.001	
P_0	mM	5.5	Fang et al. (2004)
α'	cm^2/h	0.001	Casciari et al. (1988), Jiang et al. (2005)
γ	1/h	0.002	Drasdo and Höhme (2005), Jiang et al. (2005)
γ_{as}	1/h	200	Drasdo and Höhme (2005), Freyer and Sutherland (1985)
β_{as}	1/h	5	Kole et al. (1999)
α	cm^2/h	8.3×10^{-8}	Chaplain and Matzavinos (2006), Swanson et al. (2003)

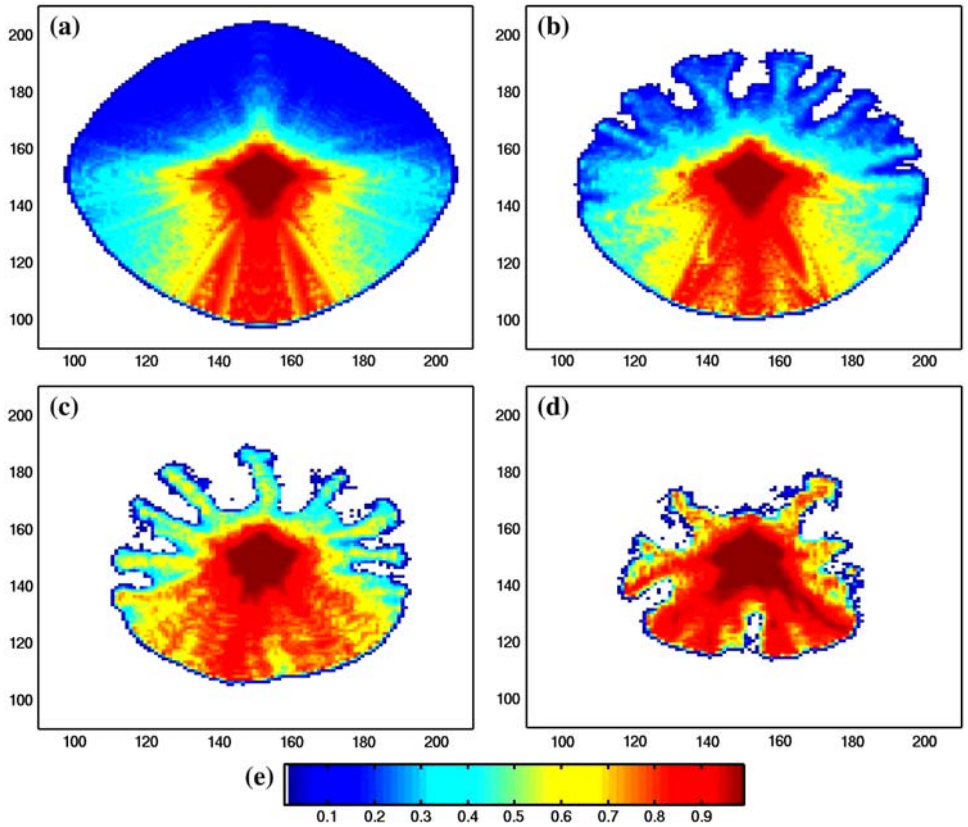

Fig. 1 Snapshots of a growing tumor, 60 days after seeding. **a** No shedding. In the rest of the panels, shedding occurs with a probability $\chi = 0.5$. All cancer cells become detached from the chosen sites ($F = 1$). The corresponding thresholds are **b** $L = 0.3$, **c** $L = 0.7$, and **d** $L = 1.2$. In **e** we show the color scheme utilized. *Darkest red* corresponds to $c(\mathbf{i}) + d(\mathbf{i}) = 1$ (all cells are either cancerous or dead)

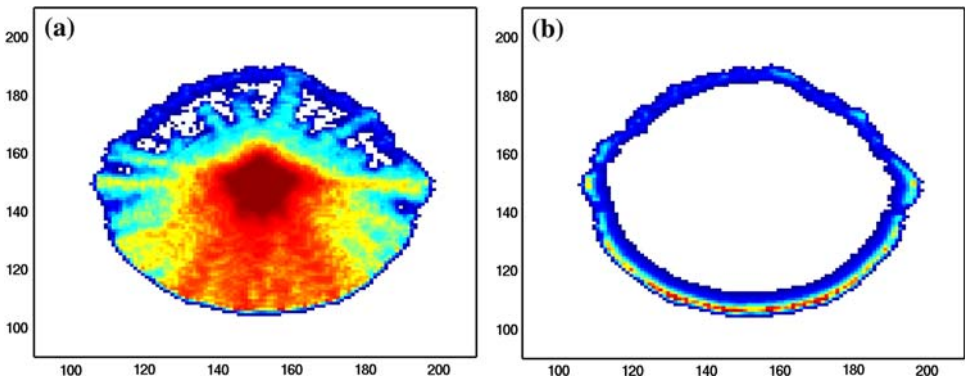

Fig. 2 Snapshots of a growing tumor, including **a** live and necrotic cells and **b** only live cells. The "bridge" is composed almost exclusively of live cells, while the "branches" are formed mostly of necrotic cells. Here $t = 60$ days, $t_0 = 11$ days, $L = 0.7$, $\chi = 0.5$, and $F = 0.7$. The *color scheme* is the same as that used in Fig. 1

that the growth of $M(t)$ is faster than linear. The exception is the large distance between the curves for $t = 40$ and $t = 45$ days in Fig 4; this increased distance corresponds to a change in the $M(t)$ growth rate and the onset of the quadratic regime (this will be discussed below).

The cumulative number of shed cells contains a plateau as a function of the threshold L. As Fig. 5 shows, this number grows monotonically as a function of L up to $L \approx 1.65$, remaining approximately independent of L between this value and $L \approx 2.3$. For higher values of L, M decreases sharply, suggesting that the ease with which cells detach is strongly limiting tumor growth. For $L > rsim2.5$, shedding stops after $t \approx 35$ days, indicating that the MTS has entered a latent stage, where most cells are necrotic and the few remaining viable cells are quiescent. Next we consider the cumulative number of shed cells as a function of time. Our results (see Fig. 6) indicate that after a transient, and except for the highest values of the threshold L, this number grows proportionally to the second power of the time elapsed after shedding began. Note that for $L = 2.5$, $M(t)$ reaches a plateau, which is consistent with the results shown in Fig. 5.

Discussion

Our model describes cell shedding by an MTS. In vivo invasion and migration involve more complicated mechanisms, including the interaction with the extracellular

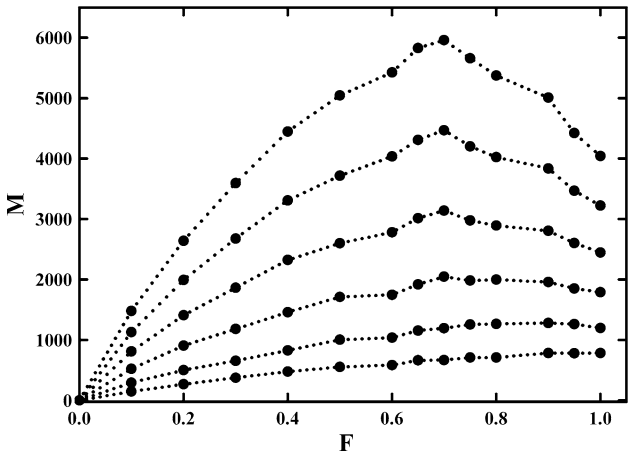

Fig. 3 Cumulative number of shed cells as a function of the detached fraction. Here $L = 0.7$ and $\chi = 0.5$. Starting from the lowest curve, the lines correspond to times beginning at $t = 35$ days and reaching up to 60 days, at 5-day intervals

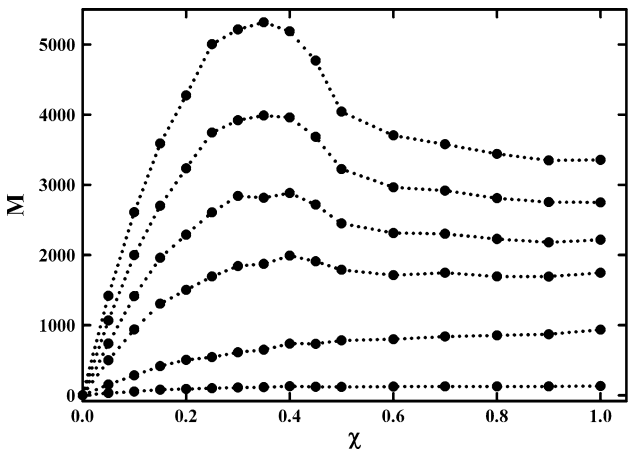

Fig. 4 Cumulative number of shed cells as a function of the shedding probability. Here $L = 0.7$ and $F = 0.5$. Starting from the lowest curve, the lines correspond to times beginning at $t = 35$ days and reaching up to 60 days, at 5-day intervals

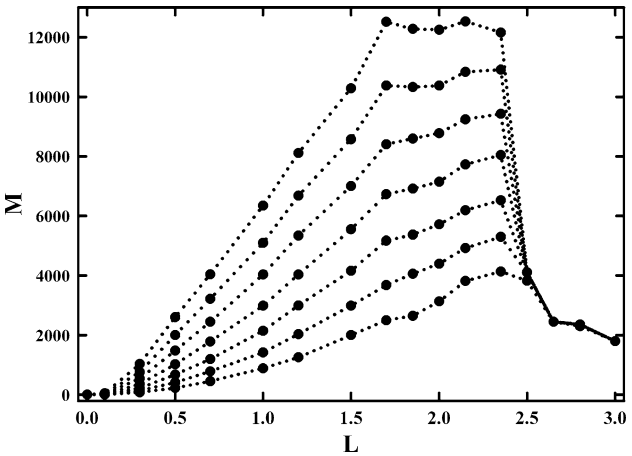

Fig. 5 Cumulative number of shed cells as a function of the shedding threshold. Here $F = 1$ and $\chi = 0.5$. Starting from the lowest curve, the lines correspond to times beginning at $t = 30$ days and reaching up to 60 days, at 5-day intervals

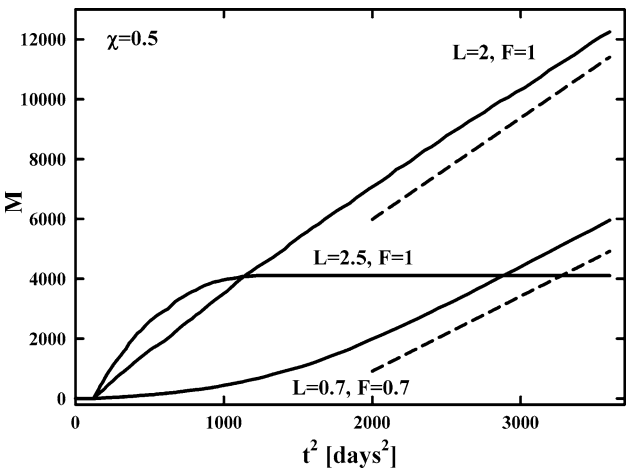

Fig. 6 Dependence of the cumulative number of shed cells with the square of the time elapsed from the moment shedding began, for the parameter values specified next to the corresponding curves. The *dashed lines* are for eye guidance only and correspond to $M(t)$ varying as $(t - t_0)^2$

matrix substrate, and the degradation and remodeling of interstitial tissue barriers (Wolf et al. 2003). Although our purpose in this paper has been more modest, there are some interesting conclusions to be drawn:

1. Shedding is strong in underfed (but not starved) tumor regions. This would agree with suggestions that hypoxia and the spatial and temporal variations in oxygen and cell nutrients may favor invasive processes (Cristini et al. 2005; Frieboes et al. 2006). However, since explicit calculations of the dependence of shedding with surface roughness are still in course, we are not yet able to make quantitative predictions. The association between roughness and shedding has also been observed by Günther et al. (2007).
2. There are optimal values of the shedding probability and the fraction of detached cells that maximize the total number of shed cells. Presumably these intermediate values occur in the case of successful metastases. The maxima of $M(t)$ at $F \approx 0.7$ (Fig. 3) and $\chi \approx 0.35$ (Fig. 4) have similar explanations: if F (or χ) is large, a high proportion of the cells located in LAEs detach and a smooth structure evolves. As a consequence, the remaining cells are mostly located in high adhesion environments and the detachment effectively decreases. The maxima in the curves tell us the parameter values at which the smoothening of the spheroid begins. If F (or χ) is small, we have a rough spheroid, but few of the cells located in LAEs detach.

3. If the shedding threshold is high ($L > rsim2.5$), almost all the new cells find themselves located in an LAE and detach. As a consequence of the intense detachment, a core formed almost exclusively by dead cells is left behind. Few viable cells are left, all of them quiescent. This is the only case where we find latency, which suggests that an inhibitor should be present if a tumor with a large number of viable cells is to go latent. The parameter L is a measure of (lack of) adhesion: A low value of L indicates that a few neighbors keep the cell from detaching, while $L = 4$ would mean that the cell detaches unless it is completely surrounded by other cancer cells. The results presented in Fig. 5 are reasonable because a low L (strong adhesion) means weak shedding, while a high L impedes growth: any new cell would detach, so that the tumor does not grow and, in the end, the number of shed cells is reduced.
4. For $L \lesssim 2.3$, temporary cancer cell structures (arches, islands) develop, mainly for values of F and χ that favor shedding, and the tumor exhibits a very rough surface (this is especially true in tumor regions where feeding is restricted).
5. A branch structure appears for a range of parameter values. When these branches emerge, the regions near the branch tops consist of multiplying cells. Most of the new cells created in the branch periphery detach, but those located in the branch interior remain, since higher adhesion hinders detachment. Eventually, the cells in the columns starve and form an irregular necrotic core.
6. In most cases, we observe that the effective radius R grows roughly linearly with time (figure not shown), and we may write $R \sim \rho t$. This is in agreement with multiple observations (Landry et al. 1982; Drasdo and Höhme 2005; Brú et al. 2003; Stein et al. 2007; Günther et al. 2007). On the other hand, since the cumulative number $M(t)$ of shed cells grows as $(t - t_0)^2$, the shedding rate must grow as $(t - t_0)$. This is proportional to the growth rate of R and hence to that of the MTS perimeter. We conclude that the shedding rate per unit area is approximately independent of time, in agreement with the observations of Freyer and Sutherland (1986b), who noticed that for EMT6/Ro spheroids, there was no correlation between the number of cells released per mm^2 of spheroid surface area per h and the spheroid diameter, in any growth condition. These authors obtained shedding rates varying from 175 to 280 cells per mm^2 per h. Indeed, we can estimate the rate per mm^2 in our simulations if we assume that our system has a thickness H corresponding to the diameter of a single cell. The lateral surface is then, approximately, $S(t) \sim 2\pi R(t)H \sim 2\pi\rho tH$. If the cumulative number of shed cells is $M(t) = c(t - t_0)^2$, then the whole system sheds cells at the rate $K(t) = 2c(t - t_0)$, and the rate per unit area is $s = K(t)/S(t) \sim c/\pi\rho H$. For instance, in the case of Fig. 1c, $F = 1$, $\chi = 0.5$, and $L = 0.7$, we obtain $c = 1.44$ cells per day^2 and $\rho = 15.5$ μm per day. By taking $H = 10$ μm, we estimate $s \approx 123$ cells per mm^2 per h, a value not too different from that obtained in (Freyer and Sutherland 1986b). This value is also intermediate between the bounds obtained for U87AE-GFR spheroids, $s_{\min} = 71$ cells per mm^2 per h and $s_{\max} = 288$ cells per mm^2 per h (Stein et al. 2007). By inspection of Fig. 5, we see that s can be several times larger than the estimate above, thus being also consistent with the results of (Stein et al. 2007) for U87WT spheroids. Of course, in a truly three-dimensional simulation, we should expect that $M(t) \sim (t - t_0)^3$ and $S(t) \sim t^2$, still corresponding approximately to a constant rate for unit area.

The model presented here can be extended to include other aspects relevant to the invasive process. A first step would be to investigate what occurs if the spheroid is immersed in a medium that can both promote and inhibit invasion, such as collagen. It is likely that a detaching cell, instead of separating completely from the tumor mass will serve as a pilot cell behind which other cells would advance into the surrounding medium, perhaps giving rise to a thin branch structure of the type observed by Kaufman et al. (2005). The model can be also applied to investigate the effects on spheroid dynamics of an inhibitory factor generated by the dead or dying cells on spheroid dynamics.

Spheroids are model systems for real cancers. Our simulational model may contribute to a better understanding of the invasive process. In particular, our simulations indicate that shedding is maximized for those values of the parameters that generate a structured spheroid surface. In general, these values (as measured by L, χ, and F) correspond to intermediate levels of cell–cell adhesion. Given that a tumor usually consists of several cell subspecies, this result suggests some experiments that could be helpful in predicting the metastatic potential of a given tumor subspecies: (a) In vitro measurements of cellular adhesion. (b) In vitro observation of spheroid roughness, which should be correlated with the adhesion results. (c) Spheroid implantation in animal models and measurement of the ratio at which cells are shed (Wyckoff et al. 2000), to confirm that the predicted effect actually occurs under in vivo conditions.

Acknowledgments This work was supported by SECyT-UNC, ANPCyT (PICT 2205/33675) and CONICET (Argentina) through Grant PIP 6311/05.

References

Brú A, Albertos S, Subiza JL, López García-Asenjo J, Brú I (2003) The universal dynamics of tumor growth. Biophys J 85:2948–2961

Casciari JJ, Sotirchos SV, Sutherland RM (1988) Glucose diffusivity in multicellular tumor spheroids. Cancer Res 48:3905–3909

Capogrosso-Sansone B, Delsanto PP, Magnano M, Scalerandi M (2001) Effects of anatomical constraints on tumor growth. Phys Rev E 64:021903

Chaplain M, Matzavinos A (2006) Tutorials in mathematical biosciences III: cell cycle, proliferation, and cancer. In: Mathematical modeling of spatio-temporal phenomena in tumor immunology. Springer, New York, pp 131–186

Condat CA, Capogrosso-Sansone B, Delsanto PP, Scalerandi M (2001) Modeling cancer growth. Recent Res Dev Biophys Chem 2:53–69

Cristini V, Frieboes H, Gatenby R, Caserta S, Ferrari M, Sinek J (2005) Morphologic instability and cancer invasion. Clin Cancer Res 11:6772–6779

Delsanto PP, Romano A, Scalerandi M, Pescarmona GP (2000) Analysis of a "phase transition" from tumor growth to latency. Phys Rev E 62:2547–2554

Drasdo D, Höhme S (2005) A single-cell-based model of tumor growth in vitro: monolayers and spheroids. Phys Biol 2:133–147

Fang J, Sullivan M, McCutchan TF (2004) The effects of glucose concentration on the reciprocal regulation of rrna promoters in plasmodium falciparum. J Biol Chem 279:720–725

Freyer JP, Sutherland RM (1985) A reduction in the in situ rate of oxygen and glucose consumption of cells on emt6/ro spheroid during growth. J Cell Physiol 124:516–524

Freyer JP, Sutherland RM (1986a) Proliferative and clonogenic heterogeneity of cells from emt6/ro multicellular spheroids induced by the glucose and oxygen supply. Cancer Res 46:3513–3520

Freyer JP, Sutherland RM (1986b) Regulation of growth saturation and development of necrosis in emt6/ro multicellular spheroids by the glucose and oxygen supply. Cancer Res 46:3504–3512

Frieboes HB, Zheng X, Sun C-H, Tromberg B, Gatenby R, Cristini V (2006) An integrated computational/experimental model of tumor invasion. Cancer Res 66:1597–1604

Greenspan HP (1972) Models for the growth of a solid tumor by diffusion. Stud Appl Math 52:317–340

Greenspan HP (1976) On the growth and stability of cell cultures and solid tumors. J Theor Biol 56:229–242

Günther S, Ruhe C, Derikito MG, Böse G, Sauer H, Wartemberg M (2007) Polyphenols prevent cell shedding from mouse mammary cancer spheroids and inhibit cancer cell invasion in confrontation cultures derived from embrionic stem cells. Cancer Lett 250:25–35

Hamilton G (1998) Multicellular spheroids as an in vitro tumor model. Cancer Lett 131:29–34

Jiang Y, Pjesivac-Grbovic J, Cantrell C, Freyer JP (2005) A multiscale model for avascular tumor growth. Biophys J 89:3884–3894

Kaufman LJ, Brangwynne CP, Kasza KE, Filippidi E, Gordon VD, Deisboeck TS, Weitz DA (2005) Glioma expansion in collagen i matrices: analyzing collagen concentration-dependent growth and motility patterns. Biophys J 89:635–650

Kole AC, Plaat BEC, Hoekstra HJ, Vaalburg WM, Molenaar W (1999) Fdg and l-[1-11c]-tyrosine imaging of soft-tissue tumors before and after therapy. J Nucl Med 40:381–386

Landry JM, Lord EM, Sutherland RM (1982) In vivo growth of tumor cell spheroids after in vitro hyperthermia. Cancer Res 42:93–99

Menchón SA, Condat CA (2008) Cancer growth: predictions of a realistic model. Phys Rev E 78: 022901

Menchón SA, Ramos RA, Condat CA (2007) Modeling subspecies and the tumor-immune system interaction: steps toward understanding therapy. Physica A 386:713–719

Mueller-Klieser W (2000) Tumor biology and experimental therapeutics. Crit Rev in Oncol Hematol 36:123–139

Nagy JD (2005) The ecology and evolutionary biology of cancer: a review of mathematical models of necrosis and tumor cell diversity. Math Biosci Eng 2:381–418

Scalerandi M, Romano A, Pescarmona GP, Delsanto PP, Condat CA (1999) Nutrient competition as a determinant for cancer growth. Phys Rev E 59:2206–2217

Scalerandi M, Capogrosso-Sansone B, Benati C, Condat CA (2002) Competition effects in the dynamics of tumor cords. Phys Rev E 65:051918

Stein AM, Demuth T, Mobley D, Berens M, Sander LM (2007) A mathematical model of glioblastoma tumor spheroid invasion in a three-dimensional in vitro experiment. Biophys J 92:356–365

Swanson KR, Bridge C, Murray JD, E.C. Alvord J (2003) Virtual and real brain tumors: Using mathematical modeling to quantify glioma growth and invasion. J Neurol Sci 216(1):1–10

Wolf K, Mazo I, Leung H, Engelke K, von Andrian UH, Deryugina EI, Strongin AY, Bröcker EB, Friedl P (2003) Compensation mechanism in tumor cell migration: mesenchymal-amoeboid transition after blocking of pericellular proteolysis. J Cell Biol 160:267–277

Wyckoff JB, Segall JE, Condeelis JS (2000) The collection of the motile population of cells from a living tumor. Cancer Res 60:5401–5404